Acta Mech Sin (2011) 27(1):36–43
DOI 10.1007/s10409-011-0412-5

RESEARCH PAPER

Analysis of regular and chaotic dynamics of the Euler–Bernoulli beams using finite difference and finite element methods

J. Awrejcewicz · A.V. Krysko · J. Mrozowski · O.A. Saltykova · M.V. Zhigalov

Received: 24 August 2010 / Revised: 18 November 2010 / Accepted: 18 November 2010

Abstract Chaotic vibrations of flexible non-linear Euler–Bernoulli beams subjected to harmonic load and with various boundary conditions (symmetric and non-symmetric) are studied in this work. Reliability of the obtained results is verified by the finite difference method (FDM) and the finite element method (FEM) with the Bubnov–Galerkin approximation for various boundary conditions and various dynamic regimes (regular and non-regular). The influence of boundary conditions on the Euler–Bernoulli beams dynamics is studied mainly, dynamic behavior vs. control parameters $\{\omega_p, q_0\}$ is reported, and scenarios of the system transition into chaos are illustrated.

Keywords Euler–Bernoulli beams · Chaos · Finite difference method · Finite element method

1 Introduction

Owing to remarkable development of aeronautics, astronautics and ship building industry, the problem of an accurate and engineering-accepted beam dynamics modeling (taking into account various boundary conditions and periodic loads) is of high importance. It is well known that the problems yielded by mechanical engineering require construction and analysis of their mathematical models. Modeling of flexible beam vibrations subjected to transversal and longitudinal periodic loads belongs to one of the most important problems of today's mechanics.

Maewal [1] studied the evolution equations of amplitudes of a harmonically simply supported beam showing existence of its chaotic vibrations. Both the Lyapunov exponents and the Lyapunov dimension of the chaotic attractors are estimated.

Ravindra and Zhu [2] studied bifurcational and chaotic behavior of axially accelerated beams in the super critical regime.

Ramu and Sankar [3] applied the Galerkin method to convert the partial differential equation governing dynamics of a pre-buckled beam into a set of ordinary differential equations. Both existence of bifurcations and chaos are illustrated and the occurred catastrophes are classified.

Wang et al. [4] analysed a flexible beam model with a bounded piezo-patches. They applied a concept of semi-active control to design a controller and the proposed control is validated numerically.

Pellicano and Vestroni [5] analysed bifurcation and chaos numerically in an axially moving beam with transverse load claiming that a few number of degree-of-freedom is sufficient to follow the beam dynamic behavior.

Taking into account the cited references (and beyond) one may conclude that today's key targets of modeling and analysis of spatial objects including a beams, plates and shells dynamics are detection and clarification of bifurcations and transitions from regular to chaotic dynamics and

J. Awrejcewicz (✉) · J. Mrozowski
Department Automation and Biomechanics,
Technical University of Łódź, Poland
e-mail: awrejcew@p.lodz.pl

A.V. Krysko · O.A. Saltykova · M.V. Zhigalov
Department of Mathematics and Modeling,
Saratov State University, Russian Federation

dynamics control via external load action (a part of this research direction has been already reported in Refs. [6-8]).

This work aims at the comparison of the results obtained by two different methods of mathematical modeling, i.e. FDM and FEM, using the example of Euler–Bernoulli type flexible beams. In addition, it is shown that the rough approximation of the beam dynamics using only a few degrees-of-freedom may yield the erroneous results.

2 Problem formulation

As it has been already mentioned, in this work the transversal Euler–Bernoulli beam vibrations subjected to various boundary conditions are studied. A physical beam model under investigation is shown in Fig. 1. Since the general approach yielding a mathematical model of transversal Euler–Bernoulli beam vibrations is widely described in classical books devoted to spatial objects dynamics (see, for instance monographs [9, 10]), here only the key steps of the beam vibrations derivation are given.

The Cartesian coordinates system xoz (Fig. 1) is introduced, and then in the space $\Omega = \{x \in [0,a]; -h \le z \le h; -b/2 \le y \le b/2\}$ a thin elastic beam with its middle surface deformation $\epsilon_x = \partial u/\partial x + (\partial w/\partial x)^2/2$ is studied. Here $w(x,t)$ denotes beam deflection, and $u(x,t)$ is the middle surface displacement along the ox axis. It is assumed that owing to the Euler–Bernoulli hypothesis a normal to the beam middle surface is still normal after the beam deformation: $\varepsilon_{xx} = \varepsilon_x - z\partial^2 w/\partial x^2$, where ε_x is the middle surface deformation, $N_x = \int_{-h}^{h} \sigma_{xx} \mathrm{d}z$ is the longitudinal force, and $M_x = \int_{-h}^{h} \sigma_{xx} z \mathrm{d}z = -\dfrac{(2h)^3}{12E} \cdot \dfrac{\partial^2 w}{\partial x^2}$ denotes the torque.

The dynamic governing equations have the following forms

$$
\begin{aligned}
&2hE\left[\frac{\partial^2 u}{\partial x^2} + L_3(w,w)\right] - (2h)\frac{\gamma}{g}\frac{\partial^2 u}{\partial t^2} - 2hd_2\frac{\gamma}{g}\frac{\partial u}{\partial t} = 0,\\
&2hE\left[L_1(u,w) + L_2(w,w) - \frac{(2h)^2}{12}\frac{\partial^4 w}{\partial x^4}\right] + q\\
&\quad -2h\frac{\gamma}{g}\frac{\partial^2 w}{\partial t^2} - 2hd_1\frac{\gamma}{g}\frac{\partial w}{\partial t} = 0,
\end{aligned}
\tag{1}
$$

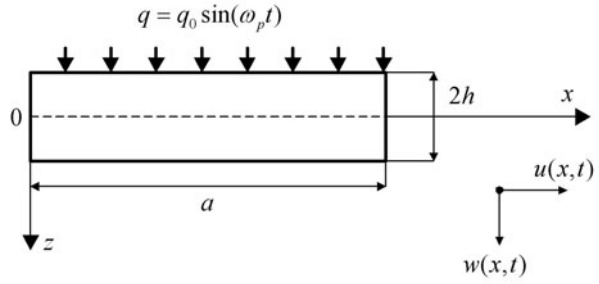

Fig. 1 The investigated beam

where the following nonlinear operators are introduced

$$
\begin{aligned}
L_1(u,w) &= \frac{\partial^2 u}{\partial x^2}\frac{\partial w}{\partial x} + \frac{\partial u}{\partial x}\frac{\partial^2 w}{\partial x^2},\\
L_2(w,w) &= \frac{3}{2}\frac{\partial^2 w}{\partial x^2}\left(\frac{\partial w}{\partial x}\right)^2,\\
L_3(w,w) &= \frac{\partial^2 w}{\partial x^2}\frac{\partial w}{\partial x}.
\end{aligned}
$$

Furthermore, the following notation is applied: d_1, d_2 are dissipation coefficients; $q = q(x,t)$ is transversal load; E is Young's modulus; ρ, γ are density and weight density, respectively, and g is acceleration of gravity. The following non-dimensional variables are introduced

$$
\begin{aligned}
&\overline{w} = \frac{w}{(2h)}, \quad \overline{u} = \frac{ua}{(2h)^2}, \qquad \overline{x} = \frac{x}{a},\\
&\lambda = \frac{a}{(2h)}, \quad \overline{q} = q\frac{a^4}{(2h)^4 E}, \quad \overline{t} = \frac{t}{\tau},\\
&\tau = \frac{a}{c}, \qquad c = \sqrt{\frac{Eg}{\gamma}}, \qquad \overline{d}_i = d_i\frac{a}{c}, \quad i = 1,2,
\end{aligned}
\tag{2}
$$

where all introduced quantities with bars are non-dimensional and correspond to those without bars and being earlier introduced (for instance, $\overline{w}$ and $\overline{u}$ are transversal and longitudinal beam displacements, respectively; $\overline{x}$ is beam non-dimensional length; $\overline{t}$ is non-dimensional time; $\overline{d_i}$ denote non-dimensional damping factors).

Taking into account Eq. (2), system (1) takes the form

$$
\begin{aligned}
&\frac{\partial^2 u}{\partial x^2} + L_3(w,w) - \frac{\partial^2 u}{\partial t^2} - d_2\frac{\partial u}{\partial t} = 0,\\
&\frac{1}{\lambda^2}\left[L_2(w,w) + L_1(u,w) - \frac{1}{12}\frac{\partial^4 w}{\partial x^4}\right] - \frac{\partial^2 w}{\partial t^2}\\
&\quad -d_1\frac{\partial w}{\partial t} + q = 0,
\end{aligned}
\tag{3}
$$

where overbars denoting dimensionless quantities are omitted.

The following boundary conditions at the beam ends are attached to Eq. (3).

Problem 1: "clamping–clamping"

$$
\begin{aligned}
&w(0,t) = w(a,t) = u(0,t) = u(a,t)\\
&\quad = \frac{\partial w(0,t)}{\partial x} = \frac{\partial w(a,t)}{\partial x} = 0.
\end{aligned}
\tag{4}
$$

Problem 2: "hinge–hinge"

$$
\begin{aligned}
&w(0,t) = w(a,t) = u(0,t) = u(a,t) = 0,\\
&M_x(0,t) = M_x(a,t) = 0.
\end{aligned}
\tag{5}
$$

Problem 3: "hinge–clamping"

$$
\begin{aligned}
&w(0,t) = w(a,t) = u(0,t) = u(a,t) = 0,\\
&M_x(0,t) = 0, \qquad \frac{\partial w(a,t)}{\partial x} = 0.
\end{aligned}
\tag{6}
$$

Problem 4: "hinge–free"

$$w(0,t) = M_x(0,t) = u(0,t) = 0,$$
$$M_x(a,t) = N_x(a,t) = Q_x(a,t) = 0. \tag{7}$$

In the case of clamping–clamping conditions, both beams defection and beam longitudinal displacements on its ends are equal to zero, as well as tangents to the beam slope at its ends are equal to zero.

In the case of hinge–hinge boundary conditions, the transversal and longitudinal beam end displacements as well as the bending moments M_x on the beam ends are equal to zero.

In the case of hinge–clamping conditions, both transversal and longitudinal beam end defections are equal to zero. In addition, the bending moment on the beam left edge is equal to zero, whereas the beam slope at its right edge is equal to zero.

Finally, in the case of hinge–free conditions, both transversal and longitudinal left beam end displacements are equal to zero. In addition, the bending moment M_x is equal to zero at both beam ends, whereas the longitudinal force N_x and transversal force Q_x are equal to zero at the right beam end.

Additionally, the following initial conditions are attached to Eq. (3) through Eq. (7)

$$w(x,t)\Big|_{t=0} = \frac{\partial w(x,t)}{\partial t}\Big|_{t=0} = u(x,t)\Big|_{t=0} = \frac{\partial u(x,t)}{\partial t}\Big|_{t=0} = 0. \tag{8}$$

3 Numerical solution and beam stability

Investigation on nonlinear vibrations of constructions with various dynamic states (regular and/or chaotic) requires highly accurate computational algorithms and implementation of numerical methods. Since analytical methods devoted to the analysis of non-linear models in general do not exist at all, the only way is to apply various numerical approaches for verification of reliability of the results obtained. In this work, various numerical approaches are applied, namely direct one (FDM) and variation one (FEM) in the Bubnov-Galerkin form. A comparison is made for various boundary conditions and for various dynamic regimes. In all investigated cases the beam geometric and physical parameters are taken the same.

4 FDM with approximation $O(c^2)$

The infinite dimensional problem Eq. (3) to Eq. (8) can be reduced to the finite dimensional one via the finite difference method with second order approximation $O(c^2)$. Namely, at each mesh node the following system of ordinary differential equations is obtained

$$\begin{aligned} L_{1,c}(w_i,u_i) &= d_1\dot{w}_i + \ddot{w}_i, \\ L_{2,c}(w_i,u_i) &= d_2\dot{u}_i + \ddot{u}_i, \end{aligned} \qquad i = 0,1,\cdots,n, \tag{9}$$

where n denotes the partition numbers regarding spatial coordinates, and the left hand sides of operators of Eq. (9) follow

$$\begin{aligned} L_{1,c}(w_i,u_i) = \frac{1}{\lambda^2}\Big\{ &-\frac{1}{12}\frac{1}{c^4}(w_{i-2} - 4w_{i-1} + 6w_i - 4w_{i+1} + w_{i+2}) \\ &+\frac{1}{2c}(w_{i-1} - w_{i+1})\frac{1}{c^2}(u_{i+1} - 2u_i + u_{i-1}) \\ &+\frac{1}{2c}(w_{i-1} - w_{i+1})\frac{1}{c^2}(u_{i+1} - 2u_i + u_{i-1}) \\ &+\Big[\frac{1}{2c}(w_{i-1} - w_{i+1})\Big]^2\frac{1}{c^2}(w_{i+1} - 2w_i + w_{i-1}) \\ &+\frac{1}{c^2}(w_{i+1} - 2w_i + w_{i-1})\Big[\frac{1}{2c}(u_{i+1} - u_{i-1}) \\ &+\frac{1}{8c^2}(w_{i-1} - w_{i+1})(w_{i-1} - w_{i+1})\Big] + q\Big\}, \end{aligned} \tag{10}$$

$$\begin{aligned} L_{2,c}(w_i,u_i) = &\frac{1}{c^2}(u_{i+1} - 2u_i + u_{i-1}) + \frac{1}{2c}(w_{i-1} - w_{i+1}) \\ &\times\frac{1}{c^2}(w_{i+1} - 2w_i + w_{i-1}). \end{aligned} \tag{11}$$

For $i = 1$, $i = n-1$ in Eq. (9) one has to take into consideration the so-called out of contour points, which are defined by the following boundary conditions: for problem 1, $w_{-i} = w_i$, whereas for problem 2, $w_{-i} = -w_i$. The following additional equations are supplemented to Eqs. (9) for problems 1–3

$$w_0 = 0, \quad w_n = 0, \quad u_0 = 0, \quad u_n = 0, \tag{12}$$

and for problem 4

$$w_0 = 0, \quad u_0 = 0, \quad M_x = 0, \quad N_x = 0, \quad Q_x = 0. \tag{13}$$

The initial conditions as Eq. (8) for the considered cases have the following form

$$\begin{aligned} w(x_i)|_{t=0} &= 0, \qquad u(x_i)|_{t=0} = 0, \\ \dot{w}(x_i)|_{t=0} &= 0, \qquad \dot{u}(x_i)|_{t=0} = 0, \end{aligned} \qquad i = 1,2,\cdots,n. \tag{14}$$

5 FEM with the Bubnov–Galerkin approximation

The defined problem by Eq. (3) to Eq. (8) is solved now via FEM. Owing to the FEM theory, in order to construct a beam element, the testing functions need to be introduced. The following four degrees of freedom $(w_1, w_2, \theta_1, \theta_2)$ are associated with the element and the following approximation polynomial is applied

$$\begin{aligned} w(x) &= a_1 + a_2x + a_3x^2 + a_4x^3, \\ \theta(x) &= -\frac{\mathrm{d}w}{\mathrm{d}x} = -(a_2 + 2a_3x + 3a_4x^2). \end{aligned} \tag{15}$$

After defining the constant values, an approximation function has the following form

$$w = \boldsymbol{N}_w\boldsymbol{W}, \tag{16}$$

where $\boldsymbol{N}_w = [1-3\xi^2+2\xi^3,\ -l\xi(\xi-1)^2,\ 3\xi^2-2\xi^3,\ -l\xi(\xi^2-\xi)]$; $\boldsymbol{W} = (w_1\ \theta_1\ w_2\ \theta_2)^{\mathrm{T}}$ is node displacement vector; $\xi = x/l$ is non-dimensional quantity (local coordinate).

Displacement approximation $u(x)$ has the following form

$$u = \boldsymbol{N}_u \boldsymbol{U}\,, \tag{17}$$

where $\boldsymbol{N}_u = [1-\xi,\ \xi]$ and $\boldsymbol{U} = (u_1\ u_2)^{\mathrm{T}}$. Applying the Bubnov–Galerkin procedure and taking into account the introduced approximations, the following equations of FEM are obtained

$$\begin{aligned} \boldsymbol{M}_1\ddot{\boldsymbol{W}} + \boldsymbol{C}_1\dot{\boldsymbol{W}} + \boldsymbol{K}_1\boldsymbol{W} &= \boldsymbol{F}_1(\boldsymbol{q}, \boldsymbol{U}),\\ \boldsymbol{M}_2\ddot{\boldsymbol{U}} + \boldsymbol{C}_2\dot{\boldsymbol{U}} + \boldsymbol{K}_2\boldsymbol{U} &= \boldsymbol{F}_2(\boldsymbol{p}, \boldsymbol{W}), \end{aligned} \tag{18}$$

where $\boldsymbol{M}_i$, $\boldsymbol{C}_i$ and $\boldsymbol{K}_i$ are the matrices of mass, damping and stiffness, respectively.

6 Numerical results

The considered beam (see Fig. 1) is subjected to the action of the following transversal load: $q = q_0 \sin(\omega_p t)$, where ω_p is the excitation angular frequency, and q_0 is its amplitude. The studied system is dissipative, and the damping coefficients denoted by d_1 and d_2 correspond to deflection w and displacement u, respectively.

Next, the beam dynamics and stability are studied numerically. Any method of beam partition is allowed to approximate PDEs by ODEs. Integration of the latter ones can be divided into two groups, i.e. explicit and implicit methods. The explicit methods are mainly realized via the Runge–Kutta schemes, and they are sufficient to solve our beam problem. It is mainly motivated by an observation that the considered Cauchy problem does not belong to stiff one, since in the eigenvalues frequency spectrum of the Bernoulli–Euler type equations there are no frequencies differing in the order of magnitude (see for instance considerations in Ref. [11]).

In order to verify the validity and accuracy of beam vibration simulations, both mentioned methods (FEM and FDM) are applied in problem 4, and the following fixed damping coefficients: $d_1 = 1$, $d_2 = 0$, where $\omega_p = 5.1$ is the excitation frequency, and $\lambda = a/(2h) = 50$ denotes the relative beam length. The beam is subjected to the harmonic load action with the amplitude q_0. The computation step regarding spatial coordinate equals s and time step is Δt. Both of them are yielded by the Runge principle. The stated problem is solved for beam partitions $n = 40$, $s = 1/40$, and with time step $\Delta t = 3.905\,2 \times 10^{-3}$. In order to compare the numerical results, power spectra and time histories (signals) $w(t)$ are reported in Fig. 2 for $q_0 = 100$ (it corresponds to regular dynamics), and for $q_0 = 32\,200$ (it corresponds to chaotic dynamics). Obtained ODEs are solved numerically using the fourth order Runge–Kutta method in all cases considered.

From Fig. 2 one may conclude that signals obtained via FEM and FDM practically coincide for the case of regular dynamics. In the case of chaotic dynamics, a signal produced by FDM is slightly delayed in comparison to that produced by FEM and possesses smaller amplitude. Frequency power spectra of vibrations practically either coincide in the case of regular dynamics or are close to each other in the case of chaotic dynamics. Hence, owing to the results included in Fig. 2, the results obtained via the FEM and FDM methods are reliable for either regular or chaotic beam dynamics analysis.

In order to investigate beams dynamics driven by harmonic loads, a special program package has been developed enabling construction of vibration type charts vs. control parameters $\{\omega_p, q_0\}$. For instance, in order to construct a chart with the resolution of 200×200 points, one needs to solve a problem of dynamics, to analyse frequency power spectrum and finally to compute the Lyapunov exponents for each choice of the control parameters. The developed algorithm also enables separation of the periodic dynamic zones, the Hopf bifurcation zones, quasi-periodic zones, as well as chaotic zones.

In Fig. 3, the vibration type charts vs. the control parameters $\{\omega_p, q_0\}$ for problem 4 are reported. Charts are constructed either with the application of FEM or FDM with the following fixed parameters $d_1 = 0.1$, $d_2 = 0$ for the beam length partition $n = 40$, and for the beam relative length $\lambda = a/(2h) = 50$. The excitation frequency changes from $\omega_0/2$ (chart I) to $3\omega_0/2$ (chart III), where ω_0 (chart II) denotes free frequency of the associated linear system (for problem 4 there is $\omega_0 = 5.1$). A maximal excitation amplitude corresponds to the beam deflection of $5(2h)$, and the charts are built with resolution 300×300.

Analysis of the obtained vibration type charts also supports reliability of the results obtained for various vibration regimes. Observe that the zones of chaotic vibrations vs. frequency obtained via FEM are wider than those obtained via FDM, whereas they coincide regarding the amplitude of vibrations. In order to get a vibration character chart vs. control parameters with resolution 300×300, it has to carry out 9×10^4 computational variants have to be carried out. In the case of FEM, the computational time increases about 1.5 time comparing to the FDM application (for $n = 40$). The legend introduced in Fig. 3, regarding vibration type, is also used further.

In order to confirm reliability of the results obtained for other types of boundary conditions, in Fig. 4 scales of vibration type beam character depending on the excitation amplitude $q_0 = 0.6 \times 10^4$ and for one value of ω_p are reported, and also dependences $w_{\max}(q_0)$ are shown.

The problems are solved for the following parameters: $d_1 = 1$, $d_2 = 0$, $\lambda = a/(2h) = 50$, $\omega_p = 6.9$, and beam partition regarding spatial coordinate $n = 40$.

It is shown in Fig. 4 how the boundary conditions essentially influence the system dynamics. For problem 1, the

beam exhibits periodic and bifurcation type dynamics (either for FDM or for FEM). In this case there is no transition to chaotic dynamics. In graph $w_{\max}(q_0)$ sudden jumps do not occur, and the function is smooth. In problem 2, chaotic zones matched with bifurcation zones could be observed, but periodic dynamics is not exhibited. A function presenting maximal deflection vs. excitation amplitude is smooth only at the beginning (for $q_0 = 1\,000$), where sudden jumps of $w_{\max}$ are not observed. Transition of the system from periodic to chaotic vibrations and vice versa, is characterized by sudden changes of $w_{\max}$ even for a small change of the excitation amplitude, and this is understood as stability loss of the system dynamics.

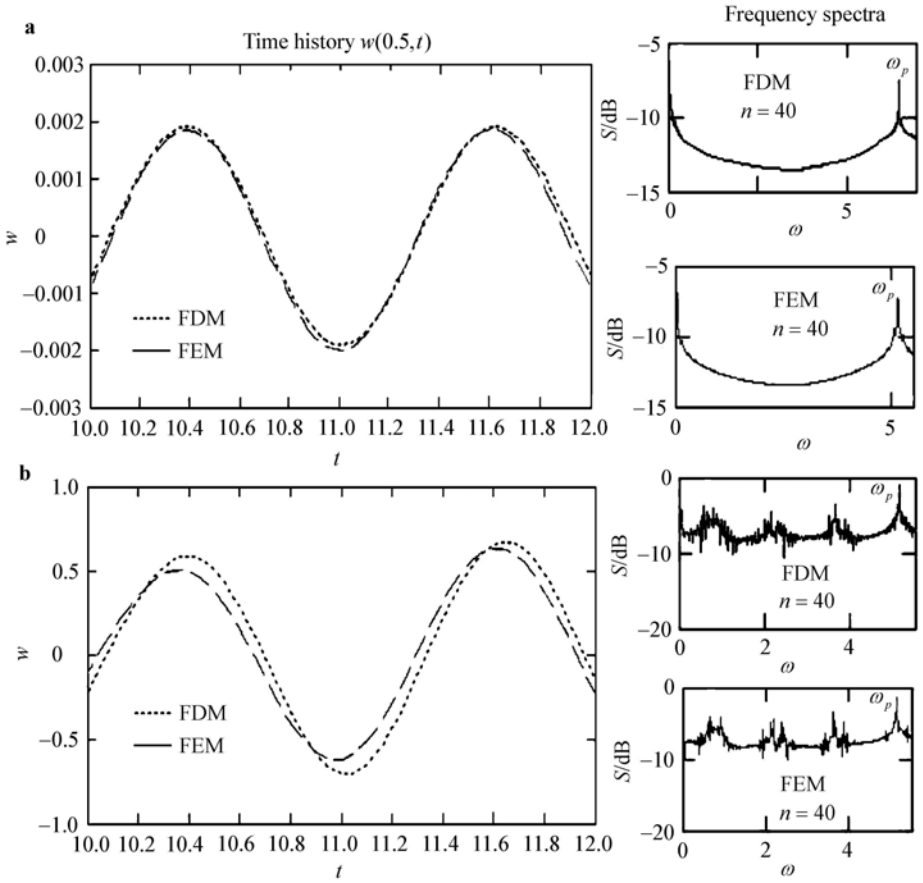

Fig. 2 Time history and frequency spectra of beam dynamics in **a** Regular ($q_0 = 100$) and **b** Chaotic ($q_0 = 32\,200$) regimes

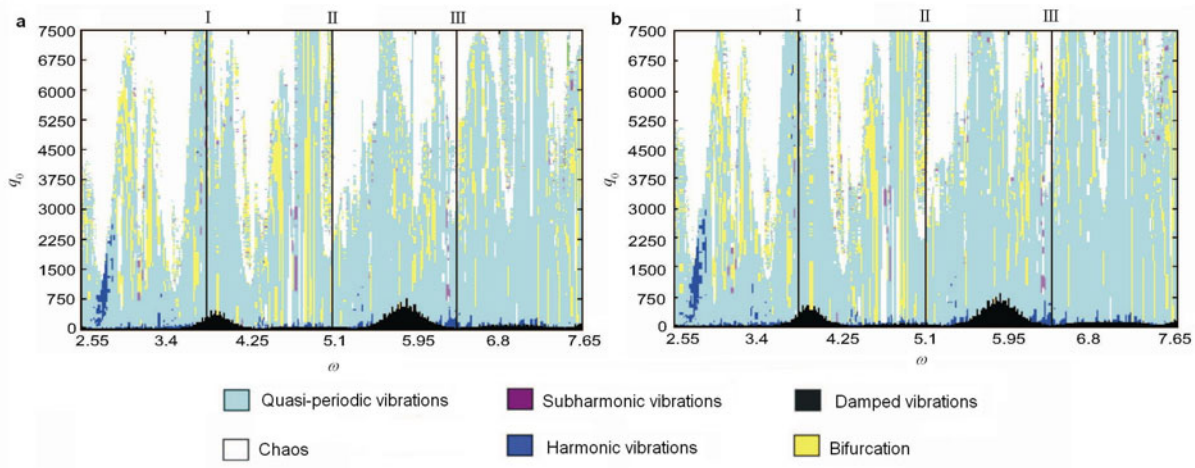

Fig. 3 Beam vibrations-type charts using **a** FDM and **b** FEM

In the case of non-symmetric boundary conditions (problem 3), the system transition into chaotic state occurs for $q_0 > 2.5 \times 10^4$ could be observed. For the given boundary conditions, the periodic dynamics occurs for $q_0 \in (1.1 \times 10^4,\ 2.5 \times 10^4)$. It is remarkable that within beam chaotic regime in the graph $w_{\max}(q_0)$ not only sudden jumps appear but also the functions are discontinuous.

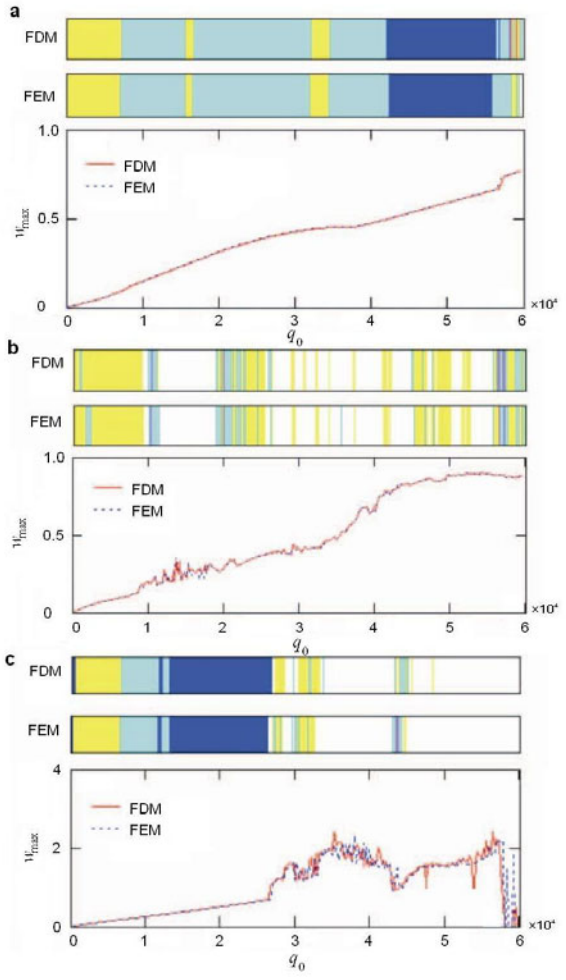

Fig. 4 Beam vibration regimes (color corresponds to that in Fig. 3) and $w_{\max}(q_0)$ for **a** Problem 1; **b** Problem 2; **c** Problem 3

7 Further results and concluding remarks

As the earlier results of local chaos investigations show, there are a few typical transition scenarios leading a dynamic system from periodicity into chaos, which sometimes are also combined. On the other hand, as it will be shown further, such transitions, however understood globally, may differ for the same system (here beam) for various boundary conditions. Four typical transitions are well understood, namely the Landau–Hopf scenario, the Ruelle–Takens–Newhouse scenario, the Feigenbaum scenario and the Pomeau–Manneville scenario (see monograph [8] for details and references therein).

Below, a beam scenario of transition into chaos for problem 2 are in vestigated and defined. The numerical investigation is carried out by two methods: FEM and FDM. Figure 5 shows the fundamental steps helping in scenario detection.

An increasing amplitude of excitation causes the occurrence of two independent frequencies (quasi-periodicity), which are evidenced by FEM and FDM, and their estimated values are the same. A further increase of the excitation amplitude causes the occurrence of linear combinations of the earlier mentioned frequencies ω_p, ω_1, ω_2.

For example, study the system behavior for $q_0 = 11\,000$ applying FDM. It is remarkable that the system dynamics is governed by a linear combination of frequencies ω_p, ω_2, ω_4. The following three frequency groups are distinguished: ω_4, ω_9, ω_7 are the first group, where frequency values differ by the amount of frequency ω_4; ω_1, ω_{10}, ω_2, ω_{11} are the second group, where the frequencies differ from each other either by ω_4, or by $2\omega_4$; ω_8, ω_5, ω_3, ω_p are the third group, where the linear combination of frequencies is preserved. Observe that an analogous system behavior is also monitored for $q_0 = 8\,700$ in the case of FEM application.

A further increase of q_0 yields more evident changes of the earlier mentioned frequencies, and finally all of the frequencies become linearly dependent. For $q_0 = 20\,000$ (FDM) and for $q_0 = 19\,900$ (FEM) all frequency distances are equal and the difference between two neighbourhoods once achieves 1.062. Observe that for $q_0 = 100$, in a frequency power spectrum, only frequency of excitation $\omega_p = 6.9$ is exhibited. An increase of the amplitude of external excitation causes variation of frequencies. The mentioned frequencies again appear and disappear. As a result, in the frequency spectra, either for FDM or for FEM, one may distinguish six linearly independent groups of frequencies, each group containing linearly dependent frequencies which differ by the amount of 0.29. Then, when all of the born frequencies become linearly dependent, the system dynamics is transited into chaotic state, which is clearly manifested by the system frequency spectra for $q_0 = 40\,000$ (FDM) and $q_0 = 39\,000$ (FEM).

Finally, taking into account the previous description and comments regarding the scenario of transition of our beam into chaotic dynamics monitored via FEM and FDM, the detected scenario fits to the well known Ruelle–Takens–Newhouse scenario, where in the latter classical case the transition is realized via two independent frequencies and their linear combinations.

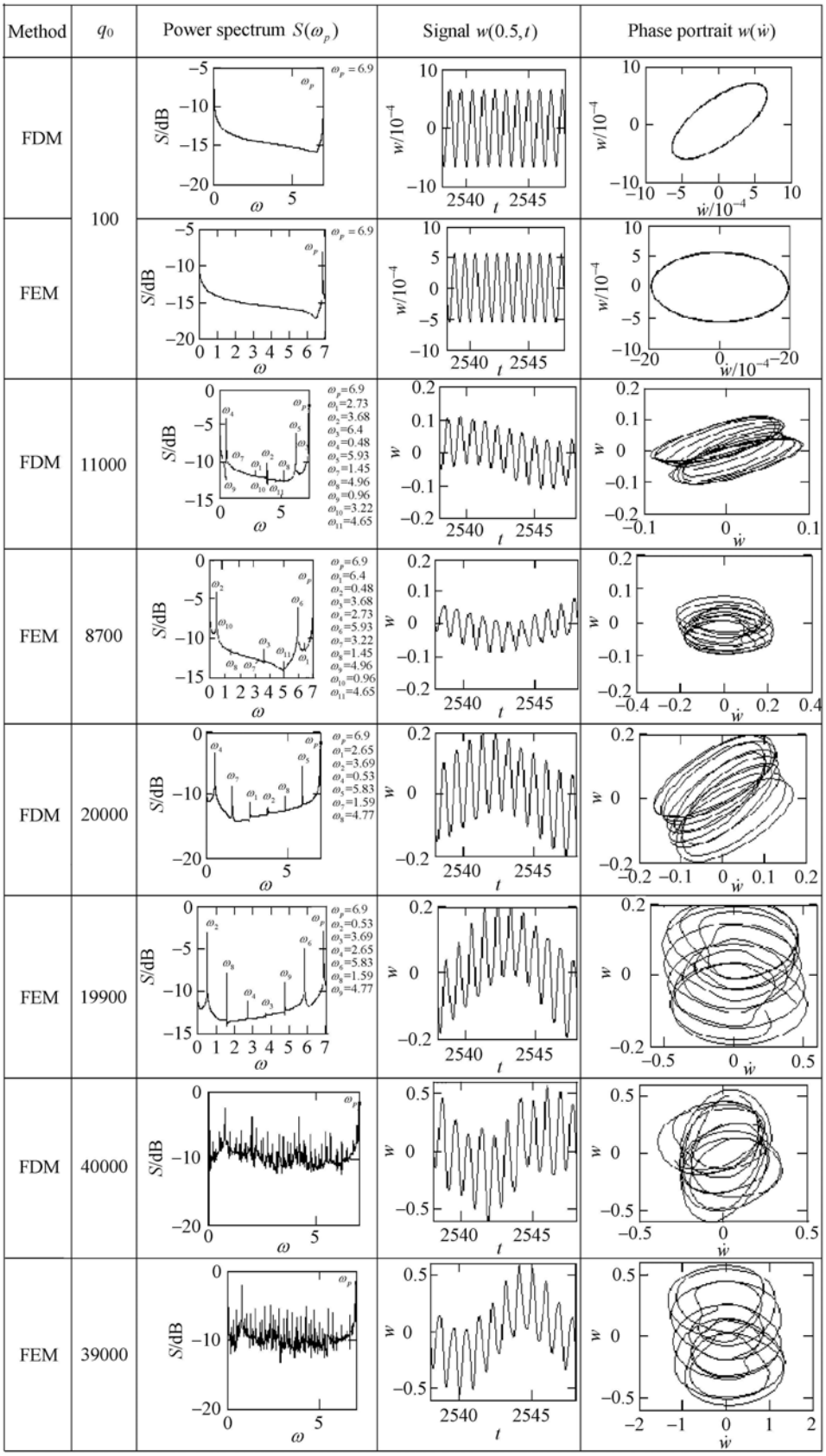

Fig. 5 Power spectra, time histories and phase portraits of beam dynamics

References

1 Maewal, A.: Chaos in a harmonically excited elastic beam. J. of App. Mech. **53**(3), 333–625 (1986)
2 Ravindra, B., Zhu, W.D.: Low dimensional chaotic response of axially accelerating continuum in the supercritical regime. Arch. Appl. Mech. **68**(3-4), 195–205 (1998)
3 Ramu, A.S., Sankar, T.S., Ganesan, R.: Bifurcations, catastrophes and chaos in a pre-buckled beam. Int. J. of Nonl. Mech. **29**(3), 449–462 (1994)
4 Wang, D., Guo, Z., Hagiwara, I.: Nonlinear vibration control by semi-active piezo-actuator damping. JSME Int. J. Ser. C **45**(2), 442–448 (2004)
5 Pellicano, F., Vestroni, F.: Complex dynamics of high-speed axially moving systems. J. Sound Vibr. **258**(1), 31–44 (2002)
6 Awrejcewicz, J., Krysko, V.A.: Feigenbaum scenario exhibited by thin plate dynamics. Nonl. Dyn. **24**(4), 373–398 (2001)
7 Awrejcewicz, J., Krysko, V.A.: Spatial-temporal chaos and solitons exhibited by von Karman model. IJBC **12**(7), 1465–1513 (2002)
8 Awrejcewicz, J., Krysko, V.A.: Chaos in Structural Mechanics. Springer Verlag, Berlin (2008)
9 Volmir, A.S.: Nonlinear Dynamics of Plates and Shells. Nauka, Moscow (1972)
10 Virgin, L.N.: Vibrations of Axially Loaded Structures. Cambridge University Press, Cambridge (2007)
11 Krysko, V.A., Awrejcewicz, J., Saltykova, O.A., et al.: Nonlinear vibrations of the Euler–Bernoulli beam subject to transversal load and impact actions. Chaos in Structural Mechanics, Understanding Complex Systems 357–373 (2008)